PAPER

A Study of Short-Range MIMO Transmission Utilizing Polarization Multiplexing for the Simplification of Decoding

Ken HIRAGA[†a)], **Kazumitsu SAKAMOTO**[†], ***Members***, **Kentaro NISHIMORI**[††], **Tomohiro SEKI**[†], **Tadao NAKAGAWA**[†], ***Senior Members***, ***and*** **Kazuhiro UEHARA**[†], ***Fellow***

SUMMARY One of the procedures for increasing the number of multi-input and multi-output (MIMO) branches without increasing the computational cost for MIMO detection or multiplexing is to exploit parallel transmissions by using polarization multiplexing. In this paper the effectiveness of using polarization multiplexing is confirmed under the existence of polarization rotation, which is inevitably present in short-range multi-input and multi-output (SR-MIMO) channels with planar array antennas. It is confirmed that 8×8 SR-MIMO transmission system with polarization multiplexing has 60 bit/s/Hz of channel capacity. This paper also shows a model for theoretical cross polarization discrimination (XPD) degradation, which is useful to calculate XPD degradations on diagonal paths.

key words: *short-range, MIMO, polarization multiplexing, XPD, antennas, decoding*

1. Introduction

The use of a short-range multi-input and multi-output (SR-MIMO) transmission between directly facing array antennas with line-of-sight environment is an effective transmission technique for short range wireless transmission [1]–[3]. High-speed numerical operation that leads to high power consumption is inevitable for multi-input and multi-output (MIMO) transmission systems due to their high amount of calculations to be processed in real time [4]. In SR-MIMO transmission systems, the channel matrix takes a particular value and is not time-variable. This feature makes it possible for SR-MIMO to achieve maximum transmission capacity with a relatively simple decoding method such as zero forcing (ZF) which needs no channel state information (CSI) feedback [5]. As a further simplification technique, the authors previously developed a simple decoding method that helps to reduce signal processing complexity and computational cost significantly through the use of an analog RF weighting matrix circuit whose input-output characteristic is fixed [6].

One of the procedures for increasing the number of MIMO branches without increasing the computational cost for MIMO decoding or multiplexing is to exploit parallel transmissions using multiple and highly-isolated paths. Realization of such parallel transmission includes, for example, isolation enhancement by using very large element spacing in array antennas. However, this is not practical because the array antenna size becomes too large to be implemented on the wireless equipment [5]. Hence, the use of polarization multiplexing is a practical way to realize parallel transmission.

A lot of MIMO transmission systems utilizing orthogonal polarization have been proposed and studied to enhance MIMO transmission performance [7], [8], especially in outdoor scenarios [9], [10]. In order to apply polarization multiplexing to SR-MIMO transmission systems, we have to consider the polarization rotation that leads to degradation of cross polarization discrimination (XPD) and polarization loss. The mechanism of these degradations is shown in the next section. Hence, SR-MIMO channel models with polarization rotation have to be employed to design such transmission systems.

So far, a number of studies that model and analyze the SR-MIMO transmission channel have been reported [11]–[13]. However, none of them clarified a method for modeling polarization rotation in the SR-MIMO channel. Furthermore, no studies had been made on applying a dual-polarized antenna to SR-MIMO transmission until a study we reported [14]. In this study we measured the performance of SR-MIMO transmission using dual-polarized antennas with the aim of miniaturizing antennas. We did not, however, describe the modeling of polarization rotation in the SR-MIMO channel or the performance of polarization multiplexing for reducing the computational cost of MIMO decoding.

This paper presents the effectiveness of polarization multiplexing that utilizes isolation between two orthogonal polarization paths in an SR-MIMO transmission channel, from which significant polarization rotations and XPD degradations arise. In Sect. 2, a formulated model of an SR-MIMO channel with a cross dipole antenna is introduced and the mechanisms of polarization rotation and XPD degradation caused purely by polarization rotation in an SR-MIMO channel are described in closed-form expressions. In Sect. 3, SR-MIMO transmission channels are analyzed by using electromagnetic simulation. Rectangular array antennas that comprise dual-polarized rectangular microstrip antenna elements are discussed because such antennas are suitable for actual implementations and fabrications in microwave bands or millimeter wave bands.

Throughout the simulations channel capacities are calculated and compared between two configurations of SR-

Manuscript received March 28, 2013.
Manuscript revised August 28, 2013.

[†]The authors are with NTT Network Innovation Laboratories, NTT Corporation, Yokosuka-shi, 239-0847 Japan.
[††]The author is with the Faculty of Engineering, Niigata University, Niigata-shi, 950-2181 Japan.
a) E-mail: hiraga.ken@lab.ntt.co.jp

DOI: 10.1587/transcom.E97.B.459

MIMO transmission systems, full MIMO decoding without polarization multiplexing and individual MIMO decoding exploiting polarization multiplexing. The comparison clarifies the effective SNR (signal-to-noise ratio) range of polarization multiplexing in SR-MIMO. The same analyses based on the measurements of transmission channels are described in Sect. 4. The last section concludes the paper with a summary of key points.

2. Effects and Issues of Dual-Polarized SR-MIMO Transmission

2.1 Effects of Polarization Multiplexing in SR-MIMO

As described in the previous section, the use of dual-polarization is an effective means to reduce the computation cost for decoding in MIMO transmission systems. In this section we explain the mechanisms for simplifying MIMO decoding. For an SR-MIMO transmission channel with square planar arrays comprising dual-polarized antenna elements, an array configuration of four elements is the minimum unit in which we can observe the polarization rotation. Therefore, planar array antennas with a larger number of elements will show the effects of polarization rotation. For this reason, in this paper the minimum number of MIMO branches is set to eight, as shown in Fig. 1. Four of eight signal streams are transmitted in vertical polarization, and the rest of them are transmitted in horizontal polarization. This allotment of polarization is clearly the best from the perspective of frequency usage efficiency. In terms of array antenna configuration, however, the use of dual-polarized antenna elements in this system has the merit of halving the number of array antennas [15]. It is well known that dual-polarized antennas are effective for miniaturizing array antennas because each of their elements has the capability of two elements.

From the perspective of MIMO decoding, SR-MIMO transmission systems with polarization multiplexing fall roughly into two categories, *(a) full 8 × 8 MIMO decoding and (b) two individual 4 × 4 MIMO decodings exploiting polarization multiplexing by isolation between two orthogonal linear polarizations*.

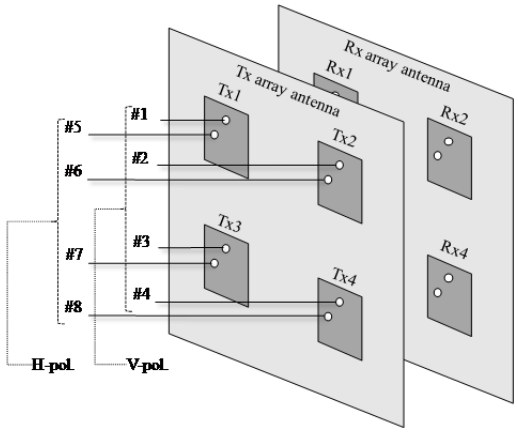

Fig. 1 SR-MIMO transmission channel with polarization multiplexing.

For the case of (a), the transmitter has a radio transmission unit for eight data streams, performs beamforming for eight antenna elements. Four of these eight streams are transmitted respectively through elements #1∼#4 in vertical polarization, and the rest of them are transmitted respectively through elements #5∼#8 in horizontal polarization. The receiver possesses the function for MIMO decoding of eight branches, which en bloc decodes eight RF (radio frequency) signals received at all of the elements. All of these RF signal powers are efficiently utilized in MIMO decoding and produce diversity effects. The system configuration for MIMO decoding is the same as that for SR-MIMO transmission with eight branches.

On the other hand, for the case of (b) two individual 4×4 MIMO decodings, the system has two transmitters, one vertically polarized and one horizontally polarized, each of them having four branches. There are two receivers, each of which performs four-branch MIMO decoding.

Here we explain the mechanism for the simplification. In operating signal processing for MIMO transmission, many matrix calculations are used for the channel estimation, weighting, MIMO detection, etc. Not only calculations, but also the CSI feedback is simplified by half. The number of elements in these matrices increases in proportion to the square of the number of branches. Hence, the computational cost increases likewise. Configuration (b) needs four receiver branches while configuration (a) needs eight. The computational cost of each receiver in (b) is one fourth of those in (a). Hence, the total computation cost of configuration (b) is half that of (a) because there are two receivers in the former.

However, in (b), the vertically-polarized receiver does not utilize all the RF signals transmitted from the horizontally-polarized transmitter and those not utilized are regarded as interference. The same is true for the horizontally-polarized receiver. In other words, unlike (a), (b) cannot exploit the diversity effect by utilizing the received power of the cross-polarization because this power is regarded as the sum of interferences.

2.2 Mechanisms of Polarization Rotation and XPD Degradations in SR-MIMO Channel

As shown in Sect. 1, when an SR-MIMO transmission channel is constructed with array antennas facing each other over a short transmission distance, polarization rotations cause cross-polarization interference and XPD degradations are expected. In the analyses reported in this section, an SR-MIMO channel comprises two directly facing rectangular array antennas whose elements are dual-polarized antenna with a vertically-polarized dipole antenna and a horizontally-polarized dipole antenna. Each array antenna has four elements. We here describe the mechanisms of the polarization rotations and XPD degradations by using the channel model illustrated in Fig. 2. In this figure, the *y*-axis

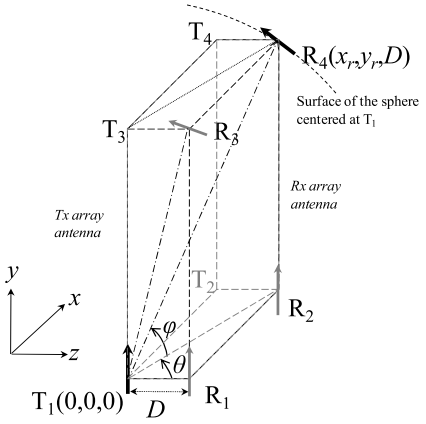

Fig. 2 Electric fields in a reception array antenna for SR-MIMO transmission.

is parallel to the vertical direction and the z-axis is parallel to the direction of transmission. Both array antennas are placed in the x-y plane. The elements of the transmitting antenna array are placed at points T_1~T_4 and those of the receiving antenna array are placed at points R_1~R_4. The receiving antenna element at R_1 directly faces the transmitting element at T_1, i.e., there is no array antenna displacement. As the figure shows, T_1~T_4 and R_1~R_4 form a cuboid. The point T_1 is located at the origin of this coordination system. The sentences below describe the directions of polarization or electric field made at reception points R_1~R_4 by the vertically-polarized transmitting element at T_1.

Analyses in many articles, such as [16], show the electric field around a dipole antenna. In the same manner, the electromagnetic field around the transmission point T_1 will propagate in a spherical surface. The directions of the electric fields (i.e., the polarizations), in R_1~R_4 are derived as shown below.

(i) The R_1 point is located on the same x-z plane as T_1. The direction of the electric field is the same as that of T_1. In other words, only the y-component has a non-zero value.

(ii) The R_2 point is located on the same x-z plane as T_1 and so only the y-component has a non-zero value.

(iii) The R_3 point is located on the plane on which T_1, T_3, and R_1 are. The electric field vector at R_3 is on the same plane and is orthogonal to the line T_1-R_3. Hence, the electric field vector has non-zero values in the y and z components.

(iv) The R_4 point, which diagonally faces T_1, is located on the plane on which T_1, T_3, and R_2 are. Hence, the electric field vector at R_4 is on that plane and is orthogonal to the line that connects T_1 and R_4. This vector is in the φ-direction and has non-zero values in the x, y, and z components. Hence, a polarization rotation is observed here.

In discussions on wireless transmission channels, the causes of XPD degradation are generally regarded as mainly reflection or depolarization of antenna elements [17]. On the other hand, in SR-MIMO channels polarization rotation is regarded to come from the location of antenna elements, even when there is no reflection. Besides, it is clear that linear arrays without displacement will not show any polarization rotation since all transmitting and receiving antenna elements are placed in the same plane, which is orthogonal or parallel to the polarization of these antenna elements. Figure 2 illustrates such a linear-array condition where there is no polarization rotation, i.e., an SR-MIMO channel with a transmitting array comprising T_1 and T_2 and a receiving array comprising R_1 and R_2. Nevertheless, some applications will require more antenna elements than denoted in Fig. 1. In such applications, it can be well expected there will be many cases in which planar arrays including rectangular arrays have to be employed because of shape and size limitations. Hence we believe it important to investigate polarization rotation in SR-MIMO channels that comprise rectangular arrays.

2.3 Formulation of XPD Degradations in SR-MIMO Channel

This subsection describes a formulation of the effects of polarization rotation and an example of its calculation. This analysis neglects the near-field components. In other words, the transmission distance should be more than $\lambda_0/(2\pi)$. Here, λ_0 is the wavelength in the transmission channel. This analysis also neglects reflections in the transmission channel.

(i) Electric field at the reception point R_4 formed by the radiated electromagnetic field from the transmitting antenna at T_1

As described in the previous subsection, the direction of the electric field vector at the receiving antenna element is the φ-direction. When the transmitting antenna element is located at an origin in the air whose dielectric constant is 1.0, the complex amplitude of the electric field is

$$E_{r\_\boldsymbol{\varphi}} = -j60I \cdot \frac{e^{-jkR}}{R} \cdot \frac{\cos\{\frac{\pi}{2}\cos(90^\circ - \varphi)\}}{\sin(90^\circ - \varphi)}, \tag{1}$$

where R denotes the distance between the transmitting antenna and the reception point and k denotes the wavenumber at the radio frequency [18]. When the transmission power at the antenna is P_t, the current on the transmission antenna I can be expressed as below because the radiation resistance of a dipole antenna is 73.13 Ω.

$$I = \sqrt{\frac{P_t}{73.13}} \tag{2}$$

Equation (1) can be transformed in the time-domain function, $E_r(t)$.

$$\begin{aligned} E_r(t) &= \mathrm{Re}[E_{r\_\boldsymbol{\varphi}} \cdot e^{j2\pi ft}] \\ &= \frac{60I}{R} \cdot \frac{\cos\{\frac{\pi}{2}\cos(90^\circ - \varphi)\}}{\sin(90^\circ - \varphi)} \sin(2\pi ft - kR) \end{aligned} \tag{3}$$

The amplitude of the electric field is the absolute value of $E_r(t)$.

$$E_r = |E_r(t)| = \frac{60I}{R} \cdot \frac{\cos(\frac{\pi}{2}\sin\varphi)}{\cos\varphi} \tag{4}$$

The direction of the electric field can be derived geometrically from Fig. 2, where we define the unit vector $\mathbf{e_r}$ that indicates this direction.

$$\mathbf{e_r} = \begin{pmatrix} -\sin\varphi\sin\theta \\ \cos\varphi \\ -\sin\varphi\cos\theta \end{pmatrix}, \quad \text{where } \mathbf{E}_r = E_r\mathbf{e_r} \tag{5}$$

When performing the computation, angles θ and φ can be derived using the equations below. Here, the coordinates of the transmitting antenna T_1 are (x_t, y_t, z_t)= (0, 0, 0) and those of the receiving antenna R_4 are (x_r, y_r, D).

$$\begin{aligned} \theta &= \mathrm{Tan}^{-1}\left(\frac{x_r - x_t}{D}\right) \\ \varphi &= \mathrm{Tan}^{-1}\left(\frac{y_r - y_t}{\sqrt{(x_r - x_t)^2 + D^2}}\right) \\ &= \mathrm{Sin}^{-1}\left(\frac{y_r - y_t}{r}\right), \quad r = |\mathbf{R}_4 - \mathbf{T}_1| \end{aligned} \tag{6}$$

Consequently the electric field vector at R_4 is

$$\mathbf{E}_r = \frac{60I}{R} \cdot \frac{\cos(\frac{\pi}{2}\sin\varphi)}{\cos\varphi} \begin{pmatrix} -\sin\varphi\sin\theta \\ \cos\varphi \\ -\sin\varphi\cos\theta \end{pmatrix} \tag{7}$$

(ii) Reception power levels at each linear-polarized antenna element

The unit vector $\mathbf{e_r}$ indicates the direction of the electric field $\boldsymbol{E_r}$. When the unit vector $\mathbf{p}$ is defined to be indicating the polarization direction of the receiving antenna element, the value θ_p, which denotes the angle produced by vectors $\mathbf{e_r}$ and $\mathbf{p}$, is

$$\begin{aligned} \mathbf{e_r} \cdot \mathbf{p} &= |\mathbf{e_r}||\mathbf{p}|\cos\theta_p = \cos\theta_p \\ \theta_p &= \mathrm{Cos}^{-1}(\mathbf{e_r} \cdot \mathbf{p}) \end{aligned} \tag{8}$$

Here, $(\mathbf{e_r} \cdot \mathbf{p})$ denotes the scalar product of vectors $\mathrm{e_r}$ and $\mathbf{p}$. From Fig. 3, the $\boldsymbol{E_r}$ component that can be received by the vertically-polarized antenna element is

$$E_{r\_copol} = E_r|\cos\theta_p| = E_r|\mathbf{e_r} \cdot \mathbf{p}| \tag{9}$$

The receivable electric field intensity in the SR-MIMO channel, which produces polarization rotation, is expressed by using the scalar product of the electric field vector and the vector that indicates the antenna element's polarization. By using this equation we can calculate the polarization loss caused by the polarization rotation. Obviously, when the value θ_p is close to 0° or 180°, polarization loss is minimized.

On the other hand, the $\boldsymbol{E_r}$ component that can be received by the horizontally-polarized antenna element is

$$E_{r\_xpol} = E_r|\sin\theta_p| \tag{10}$$

By using this equation we can calculate the degradation of isolation for polarization multiplexing. In the computation of the SR-MIMO transmission channel matrix, depolarization by polarization rotation is calculated using these equations.

Here, reception power at an antenna with the gain G_r is derived by using the Friis equation [19].

$$P_r = \left(\frac{\lambda_0}{4\pi R}\right)^2 P_t G_t G_r = \frac{E^2\lambda_0^2 G_r}{480\pi^2} \tag{11}$$

Here G_t denotes transmitting antenna's gain and λ_0 denotes the wavelength in the transmission channel. This equation is said to be valid when the distance between the transmitting antenna element and the receiving antenna element R satisfies the condition below [19], where a is the largest linear dimension of the antenna element.

$$R > \frac{2a^2}{\lambda_0} \tag{12}$$

The theoretical value of XPD degradation is calculated by using the equations shown above. The model for the analysis is shown in Fig. 4. The analysis is based on the ray-tracing method, in which reflections and diffractions are neglected. The transmitting antenna is located at the origin (0,0,0) and comprises a vertically-polarized dipole antenna and a horizontally-polarized dipole antenna. The receiving antenna, which has the same configuration as the transmitting antenna, is located at $R_4(x_r, y_r, D)$. Here, the value of D is the transmission distance of the SR-MIMO channel, and x_r and y_r are the element spacings. Coupling between these two dipole antennas is assumed to be zero. Each antenna element has no directivity in this transmission path. In this

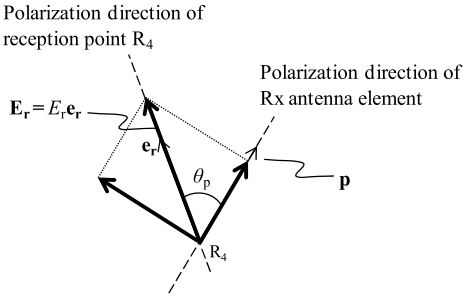

Fig. 3 Received electric field and angle of antenna element.

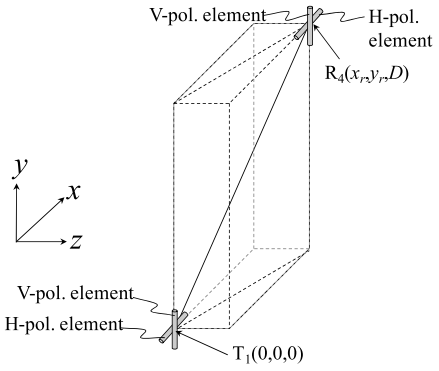

Fig. 4 XPD calculation model.

transmission system, when the transmission power is radiated from T_1's vertically-polarized antenna element, XPD can be defined in two ways. One is as the ratio of the reception power level at R_4's vertically-polarized antenna element to the reception power level at R_4's horizontally-polarized antenna element. The other is as the ratio of the reception power level at R_4's horizontally -polarized antenna element to the reception power level at R_4's vertically-polarized antenna element [17]. For the analyses in this section we use the latter because XPD values calculated using these two definitions are symmetrical about the line $y = x$ on the x-y plane.

Figure 5 shows the calculated XPD, where (a) is when $D = 1.0\lambda_0$ and (b) is when $D = 2.0\lambda_0$. Here, λ_0 is the wavelength in the transmission channel. In studies of SR-MIMO transmission systems, it is hard to expect that the element spacing of array antennas is less than $0.5\lambda_0$, the coordinate range of R_4 is $x_r > 0.5\lambda_0$, and $y_r > 0.5\lambda_0$. When $x_r = 0$, or $y_r = 0$, XPD is infinite. As in Fig. 5(a) when $D = 1.0\lambda_0$, XPD at $x_r = y_r = 1.0\lambda_0$ is 6.2 dB. With larger D, XPD at the same coordinates (x_r, y_r) takes a higher value. As in Fig. 5(b), when $D = 2.0\lambda_0$, XPD at the same (x_r, y_r) is 14.0 dB. As we can see here, XPD degradation in the SR-MIMO channel is larger when the transmission distance is smaller. Since the displacement of the array antenna is assumed to be zero in this paper, the XPD values at $x_r = y_r$ should be used. On the other hand, when there is antenna displacement, the XPD values at $x_r \neq y_r$ should be used.

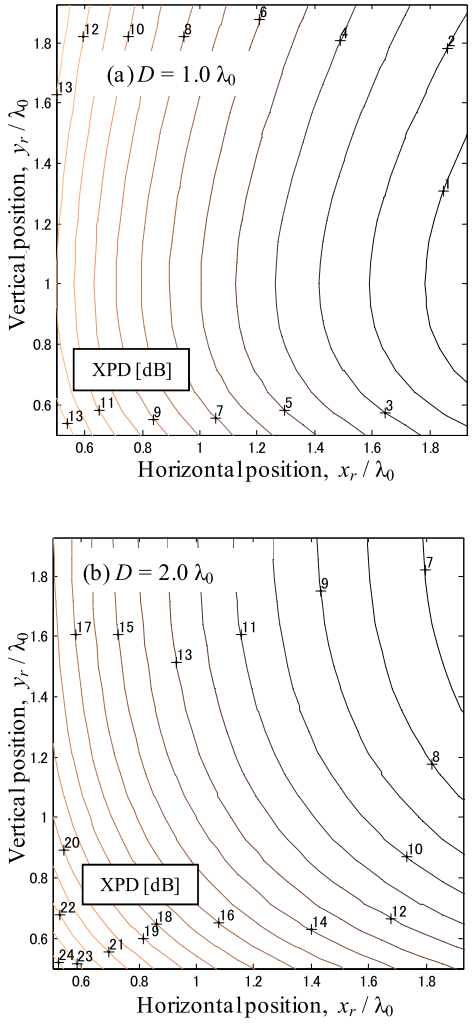

Fig. 5 Calculated XPD: (a) $D = 1.0\lambda_0$, (b) $D = 2.0\lambda_0$.

3. Channel Capacity Comparison Using Electromagnetic Simulation

By using electromagnetic simulations we obtained the channel matrix and channel capacity of the SR-MIMO channel with polarization rotation shown in the previous section in order to clarify the conditions where the polarization multiplexing is valid. The frequency was set to be 4.85 GHz. The numbers of elements were set to 4, 9 and 16. The transmission channel of the dual-polarized SR-MIMO with four antenna elements to be analyzed is illustrated in Fig. 6. Two array antennas directly face each other at distance D. It is assumed that there is no antenna displacement, a concept that we introduced in [20]. In a millimeter wave band application, 100 Gbit/s transmission with a download kiosk described in [20], antenna displacement is expected and it will affect XPD in this SR-MIMO channel with polarization multiplexing. Such applications should be implemented with potent anti-displacement mechanisms, e.g., an automatically positioned array antenna in the download kiosk and should be designed with adequate margin for the displacement. Antenna models in this paper are designed in microwave band. As scale models, these models have validity in discussions on XPD degradations and channel capacity of SR-MIMO transmission in the 60 GHz band [20]. Expected differences between microwave band and 60 GHz band include the difference in antenna efficiency caused by the dielectric coefficient and dielectric loss tangent and the

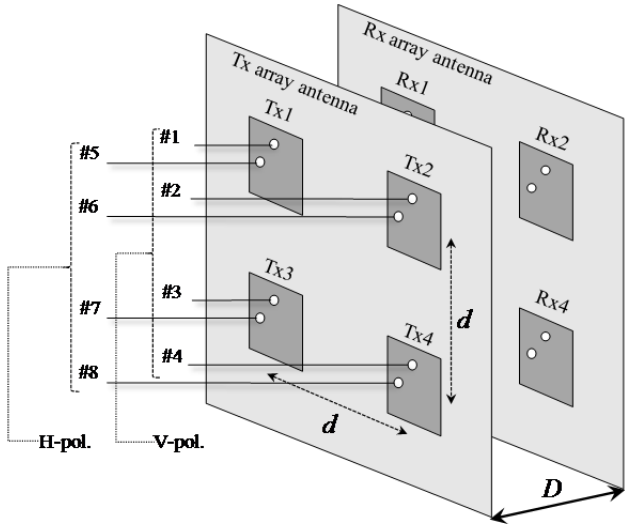

Fig. 6 Transmission channel of dual-polarized SR-MIMO with four-element array.

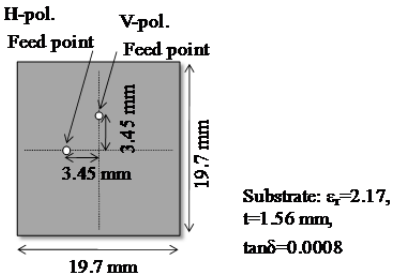

Fig. 7 Configuration of a dual-polarized antenna element.

difference in achievable manufacturing accuracy. These differences are not expected to affect XPD degradations and can be regarded as matters in fabrication, hence this paper does not present detailed discussions on them.

Each array antenna is a rectangular array whose element spacing is $d = 1.0\lambda_0$ and which comprises dual-polarized rectangular microstrip antenna elements like the one illustrated in Fig. 7. The antenna element has two feed points, one for the radiation in vertical polarization and one for that in horizontal polarization. The isolation between these points is 35.2 dB. The positions of the points are designed to be matched and to have the minimum return loss at 4.85 GHz. Unlike the dipole antenna described in the previous section, a rectangular microstrip antenna is equal to an array with two dipole antennas. The polarization rotation of a microstrip antenna is regarded as equivalent to that of a dipole antenna. The XPD degradation characteristics of both types of antennas are equivalent. On the other hand, since the directivity of a microstrip antenna is greater than that of a dipole antenna, the difference between propagation loss in a path between directly facing elements (e.g., Tx1 and Rx1 in Fig. 6) and that in a path between diagonally facing elements (e.g., Tx1 and Rx4) is larger when microstrip antennas are used. Hence the influence on channel capacity by XPD degradations in diagonally facing paths is expected to be different between the two types of antenna elements. In addition, while the isolation between the two feed points in the model of a cross dipole antenna shown in the previous section is set to be infinite, an actual rectangular microstrip antenna has finite isolation as described above.

In both array antennas, each odd-numbered port is connected to the feed point for vertical polarization and each even-numbered port is connected to the one for horizontal polarization. The numbering in this model is the same as that shown in Fig. 1.

The procedure of channel capacity analysis was as follows. First, we performed the electromagnetic simulation with the Method of Moments [21] to derive the channel matrix of the SR-MIMO channel shown in Fig. 6. Next, we calculated the channel capacities for configurations (a) and (b) shown in Sect. 2.1 by using the derived matrix. Finally, we compared the calculated capacities.

Figure 8 shows the relationship of XPD and transmission distance. This shows XPD in the path between directly facing elements (path #1, between Tx1 and Rx1) and that

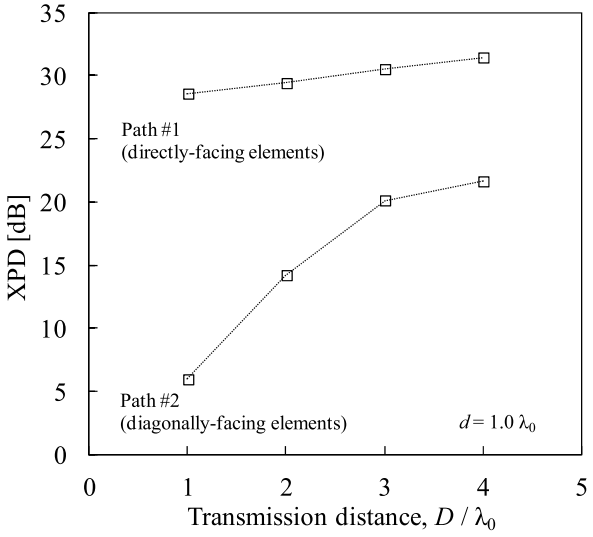

Fig. 8 XPD and transmission distance (simulated).

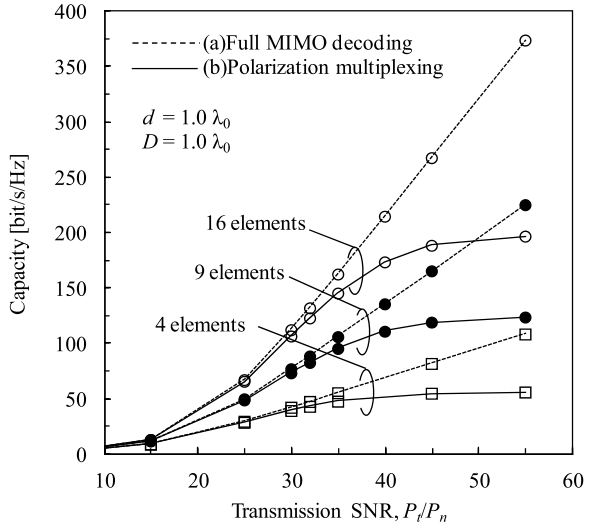

Fig. 9 Channel capacity and transmission SNR (simulated).

in the path between diagonally facing elements (path #2, between Tx1 and Rx4). As described above, the element spacing is $d = 1.0\lambda_0$. In path #1, XPD is more than 28.6 dB throughout all transmission distances, while in path #2 XPD degrades as a result of the effects of polarization rotation at smaller transmission distance. The XPD values were found to be 5.9 dB when $D = 1.0\lambda_0$ and 14.2 dB when $D = 2.0\lambda_0$; these coincide closely with the theoretical values shown in Fig. 5.

Figure 9 shows the relationship between channel capacity and transmission SNR, which is defined as the ratio of transmission power to noise at the receiver. The transmission power at each antenna element is assumed to be equal in the transmission array antenna. In calculating the channel capacity of ZF, the SNR of each stream was obtained by using the calculation shown in [22]. In calculating the channel capacity for the configuration of (b) the reception power of

the cross polarization component produced by polarization rotation (see Eq. (10)) is regarded to be noise. The element spacing is $d = 1.0\lambda_0$ and the transmission distance is $D = 1.0\lambda_0$. It is assumed that transmission beamforming is not adopted at the transmitter and that at the receiver the MIMO decoding method is ZF.

In configuration (a), channel capacity is in proportion to the SNR, while it shows saturation at 60 bit/s/Hz in configuration (b). This phenomenon is caused by depolarization. The reception power of the cross polarization component behaves as noise at the receiver even when the transmission SNR is sufficiently high. Since the same interelement spacing is applied to each number of elements, XPD degradations is large with a larger number of elements. Hence, SNR for the capacity saturation is smaller with a larger number of elements. Under these conditions ($d = 1.0\lambda_0$ and $D = 1.0\lambda_0$), achievable capacities are 60 bit/s/Hz, 123 bit/s/Hz, and 196 bit/s/Hz when the number of elements is 4, 9 and 16 respectively. For example, by simulating transmission over the 60 GHz band as described in [20], we can expect a transmission rate of over 100 Gbit/s for 90 bit/s/Hz channel capacity when the number of branches is 16 and a two-frequency channel is used in this band. To obtain the same degree of channel capacity for the present case, we have to achieve half of that capacity when using eight branches. Using configuration (b) we can obtain 60 bit/s/Hz, which is larger than half of the 90 bit/s/Hz capacity.

Under the conditions where $D = 1.0\lambda_0$ and XPD of path #2 is 5.9 dB, however, channel capacity of 60 bit/s/Hz can be obtained in the whole SR-MIMO channel. This is because the transmission loss of path #2 is larger than that of path #1 by more than 15 dB and the contribution of path #2 is much smaller than that of path #1 (this value is not shown in this paper).

However, when we use higher multilevel modulation, capacity degradation is inevitable in configuration (b).

4. Measurement of XPD and Channel Capacity

In order to ascertain the validity of the simulations described in the last section, we measured SR-MIMO channel with four element arrays. After we fabricated dual-polarized array antennas with the parameters shown in Sect. 3, we measured the channel matrices of dual-polarized SR-MIMO channels using these real array antennas, and calculated XPD and channel capacity. Figure 10 shows the fabricated dual-polarized array antenna for the receiver. The feeding points for both polarizations can be seen in this picture. It can also be seen that the antenna elements and ports are numbered in the same way as for the array antenna illustrated in Fig. 6. The SR-MIMO transmission channels were constructed by having the transmitting and receiving antennas face each other directly without displacement in the same way as shown in Fig. 6. Measurements were taken with the same frequency as that for the electromagnetic simulation described in the previous section. We used the MIMO measurement system described in [14]. The channel

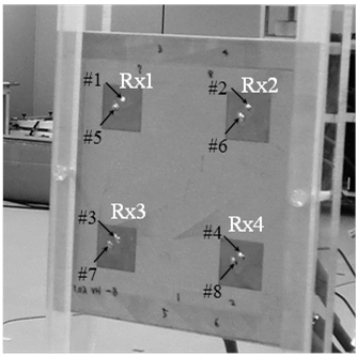

Fig. 10 Fabricated dual-polarized array antenna used for the channel measurement (receiver side).

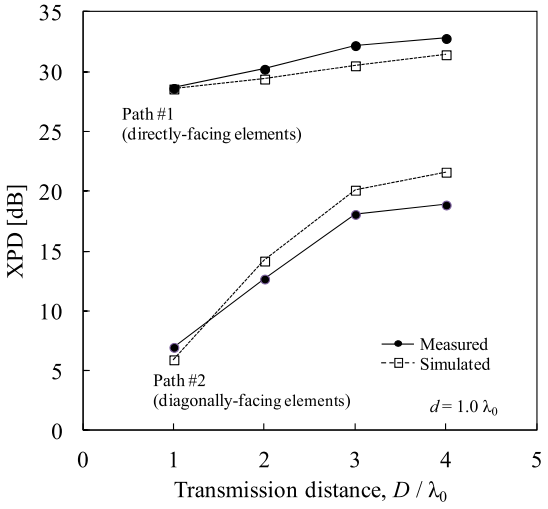

Fig. 11 XPD and transmission distance (measured and simulated).

matrix was measured by using preamble of IEEE 802.11n wireless local area network.

Figure 11 shows XPD obtained from the measured SR-MIMO channel comprising these array antennas. This plot has the same parameters as for Fig. 8. Simulated values are also plotted here to compare them with the measured values. On path #2, XPD is 6.5 dB when $D = 1.0\lambda_0$ and is 13.0 dB when $D = 2.0\lambda_0$. These values coincide closely with the simulated values shown in Fig. 8 and with the theoretical values shown in Fig. 5. These results confirm the effectiveness of the theoretical XPD degradation model described in Sect. 3.

XPD in path#1 increases as the transmission distance increases. One reason for this is regarded as coupling effect of the transmitting antenna and the receiving antenna. The coupling effects decrease when the transmission distance increases. We can see that the differences in XPD between simulation and measurement is larger with larger transmission distance. We believe that a major reason for this is the accuracy of simulation by 2.5-dimensional electromagnetic field simulator that we used [21]. In this simulation, when the transmission distance is large the accuracy in calculations of the radiation and the coupling in the direction of

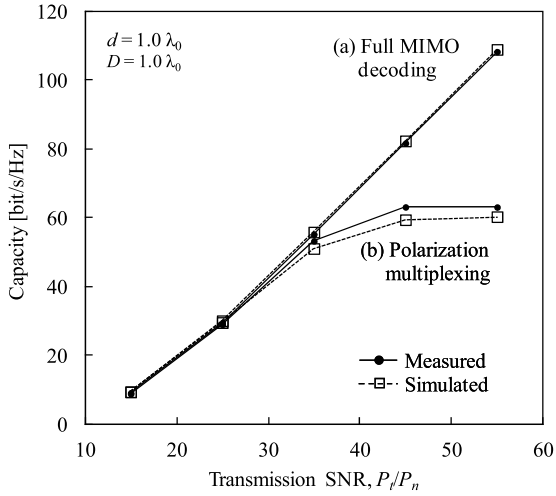

Fig. 12 Channel capacity and transmission SNR (measured and simulated).

transmission distance degrades, while the calculation accuracy in each plane is maintained.

Figure 12 shows the relationship between channel capacity and transmission SNR, which is a plot of the same parameters shown in Fig. 9 in Sect. 3. Simulated values are also plotted here to compare them with the measured values. The same trend as shown in Fig. 9 is confirmed; it shows saturation at 63 bit/s/Hz in configuration (b). However, the measured and simulated saturation values differ; as shown above, the simulated channel capacity saturates at 60 bit/s/Hz. This difference is mainly caused by the XPD difference between the measurement and the simulation. By measuring the channel matrices of SR-MIMO channels with dual-polarized antennas, we confirmed the effectiveness of using polarization multiplexing to simplify MIMO decoding. We found that when the transmission SNR is less than 35.0 dB, there is very little channel capacity difference between (a) full 8×8 MIMO decoding and (b) two individual 4×4 MIMO decodings. When the transmission SNR is 35 dB, channel capacity is 55.3 bit/s/Hz for configuration (a) and 53.2 bit/s/Hz for (b). This represents a 2.1 bit/s/Hz difference, which corresponds to an SNR difference of around 0.8 dB. Since the noise level at the receiver is set to be the same with these configurations at this transmission SNR, we believe the difference comes only from the XPD degradation stemming from the polarization rotations.

We also found that under this transmission SNR condition, effective decoding simplification can be obtained for configuration (b) without affecting channel capacity.

5. Conclusion

The effectiveness of using polarization multiplexing that halves computational cost for multiple-input and multiple-output (MIMO) decoding was confirmed under the existence of polarization rotation, a condition that is inevitably present in short-range MIMO (SR-MIMO) channels with planar array antennas. When the number of branches is eight, the achievable channel capacity utilizing polarization multiplexing is 60 bit/s/Hz. The results obtained in this paper clarify the useful range of polarization multiplexing in designing an SR-MIMO transmission system.

This paper also described a theoretical model for cross polarization discrimination (XPD) degradation we developed for dual-polarized SR-MIMO channels, which conventional studies have not shown. We believe it will prove to be useful for calculating XPD degradations on diagonal paths. Calculated results obtained with the model coincided closely with measured results for transmission distance of 1.0 or 2.0 wavelengths.

Acknowledgements

The authors would like to thank Associate Professor Naoki Honma at Iwate University for his insightful comments and suggestions on SR-MIMO technique. They also appreciate helpful support in experiments and analyses provided by Mr. Ryochi Kataoka at the Graduate School of Engineering, Niigata University. The authors also thank Mr. Masaaki Ida at NTT Advanced Technology Corporation for his helpful work on highly precise channel measurement.

References

[1] N. Honma, K. Nishimori, T. Seki, and M. Mizoguchi, "Short Range MIMO Communication," 3rd European Conference on Antennas and Propagation (EuCAP 2009), March 2009.
[2] T. Seki, K. Hiraga, K. Nishimori, and K. Nishikawa, "Experimental evaluation of high speed parallel data transmission technology for wireless repeater system," 2010 IEEE Radio and Wireless Symp., pp.304–307, Jan. 2010.
[3] T. Seki, K. Nishimori, K. Hiraga, and K. Nishikawa, "High speed parallel data transmission technology for short range wireless relay system," IEICE Technical Report, AP2009-55, July 2009.
[4] S. Yoshizawa, D. Nakagawa, N. Miyazaki, T. Kaji, and Y. Miyanaga, "LSI development of 8×8 single-user MIMO-OFDM for IEEE 802.11ac WLANs," 2011 11th International Symposium on Communications and Information Technologies, pp.585–588, 2011.
[5] K. Nishimori, T. Seki, N. Honma, and K. Hiraga, "On the transmission method for short range MIMO communication," IEEE Trans. Veh. Technol., 2011.
[6] R. Kataoka, K. Nishimori, K. Hiraga, K. Sakamoto, and T. Seki, "Simple decoding method for short range MIMO transmission," IEICE Technical Report, AP2011-173, Jan. 2012.
[7] J.P. Kermoal, L. Schumacher, F. Frederiksen, and P.E. Mogensen, "Experimental investigation of the joint spatial and polarisation diversity for MIMO radio channel," Wireless Personal Multimedia Communication 2001, Sept. 2001.
[8] N.K. Das, T. Inoue, T. Taniguchi, and Y. Karasawa, "An experiment on MIMO system having three orthogonal polarization diversity branches in multipath-rich environment," IEEE 60th Vehicular Technology Conference, 2004, p.1528, 2004.
[9] V. Eiceg, H. Sampath, and S. Catreux-Erceg, "Dual-polarization versus single-polarization MIMO channel measurement results and modeling," IEEE Trans. Wireless Commun., vol.5, no.1, pp.28–33, Jan. 2006.
[10] M.C. Mtumbuka and D.J. Edwards, "Experimental investigation of a joint dual-spaced diversity and tri-polarised MIMO system for beyond 3G," Fifth IEE International Conference on 3G Mobile Communication Technologies, 2004, p.373, 2004.

[11] I. Sarris and A.R. Nix, "On the link-level performance of MIMO systems in line-of-sight," 6th IEE International Conference on 3G and Beyond, 2005, pp.1–4, 2005.
[12] J. Jiang and M.A. Ingram, "Distributed source model for short-range MIMO," IEEE 58th Vehicular Technology Conference, 2003, pp.357–362, 2003.
[13] I. Sarris, A.R. Nix, and A. Doufexi, "High-throughput multiple-input multipleoutput systems for in-home multimedia streaming," IEEE Wireless Commun., vol.13, no.5, pp.60–66, Oct. 2006.
[14] K. Hiraga, T. Seki, K. Nishimori, and K. Uehara, "Effectiveness of short-range MIMO using dual-polarized antenna," IEICE Trans. Commun., vol.E95-B, no.1, pp.87–96, Jan. 2012.
[15] K. Hiraga, K. Sakamoto, T. Seki, T. Nakagawa, and K. Uehara, "Influences on simple decoding method for short-range MIMO by phase and amplitude errors," Proc. Commun. Conf. IEICE, B-5-105, Sept. 2012.
[16] K.A. Norton, "The propagation of radio waves over the surface of the Earth and in the upper atmosphere," Proc. Institute of Radio Engineers, vol.24, no.10, pp.1367–1387, Oct. 1936.
[17] W.L. Stutzman, "Polarization in electromagnetic systems," in Polarization in Electromagnetic Systems, pp.200–216, Artech House, Norwood, MA, 1993.
[18] S. Silver, Microwave Antenna Theory and Design., Mass. Inst., N.Y., 1949.
[19] H.T. Friis, "A note on a simple transmission formula," Proc. IRE, vol.34, no.5, pp.254–256, May 1946.
[20] K. Hiraga, T. Seki, K. Nishimori, K. Nishikawa, I. Toyoda, and K. Uehara, "Analyses of antenna displacement in short-range MIMO transmission over millimeter-wave," IEICE Trans. Commun., vol.E94-B, no.10, pp.2891–2895, Oct. 2011.
[21] Mentor Graphics. The IE3D^{TM} electromagnetic design. [Online]. http://www.mentor.com/electromagnetic-simulation/
[22] T. Ohgane, T. Nishimura, and Y. Ogawa, "Applications of space division multiplexing and those performance in a MIMO channel," IEICE Trans. Commun., vol.E88-B, no.5, pp.1843–1851, May 2005.

Ken Hiraga received the B.E., M.E., and Ph.D. degrees in electronics and information engineering from Hokkaido University, Sapporo, in 2003, 2005, and 2013 respectively. Since 2005, he has been engaged in research and development on high-speed wireless systems at Nippon Telegraph and Telephone Corporation (NTT). He received the Young Engineers Award from the IEICE in 2010 and Young Engineer Award from IEEE AP-S Japan Chapter in 2012. He is a member of IEEE and IEICE.

Kazumitsu Sakamoto received the B.E. and M.E. degrees in electrical engineering from Kyushu University, Fukuoka, Japan, in 2008 and 2010, respectively. In 2010, he joined NTT Network Innovation Laboratories, NTT Corporation and has been engaged in research on MIMO communication systems and millimeter-wave high-speed wireless systems. He is a member of IEICE.

Kentaro Nishimori received the B.E., M.E. and Ph.D. degrees in electrical and computer engineering form Nagoya Institute of Technology, Nagoya, Japan in 1994, 1996 and 2003, respectively. In 1996, he joined the NTT Wireless Systems Laboratories, Nippon Telegraph and Telephone Corporation (NTT), in Japan. He was senior research engineer on NTT Network Innovation Laboratories. He is now associate professor in Niigata University. He was a visiting researcher at the Center for Teleinfrastructure (CTIF), Aalborg University, Aalborg, Denmark from Feb. 2006 to Jan. 2007. He was an Associate Editor for the Transactions on Communications for the IEICE Communications Society from May 2007 to May 2010 and Assistant Secretary of Technical Committee on Antennas and Propagation of IEICE from June 2008 to May 2010. He received the Young Engineers Award from the IEICE of Japan in 2001, Young Engineer Award from IEEE AP-S Japan Chapter in 2001, Best Paper Award of Software Radio Society in 2007 and Distinguished Service Award from the IEICE Communications Society in 2005, 2008 and 2010. His main interests are spatial signal processing including MIMO systems and interference management techniques in heterogeneous networks. He is a member of IEEE and IEICE. He received IEICE Best Paper Award in 2010.

Tomohiro Seki received his B.E., M.E. and Dr.Eng. degrees in electrical engineering from the Tokyo University of Science, Tokyo, Japan, in 1991, 1993 and 2006, respectively. In 1993, he joined NTT and has been engaged in research on planar antennas and active integrated antennas for the millimeter-wave and microwave bands. He is currently interested in system-on-package technologies for millimeter-wave communication systems. He is a senior research engineer of NTT Network Innovation Laboratories. He received the 1999 Young Engineer Award presented by the IEICE and the 2006 Best Paper Award presented by IEICE Communications Society. He is a senior member of IEICE and a member of IEEE.

Tadao Nakagawa received the B.E. and M.E. degrees in material physics and the Dr.Eng. degree in communication engineering, all from Osaka University, Osaka, Japan, in 1986, 1988, and 1997, respectively. In 1988, he joined NTT Radio Communication Systems Laboratories, where he was involved in research and development on MMIC's, microwave synthesizers, multi-band transceivers, millimeter-wave transceivers and signal processing in optical fiber communications. Since 2009, he has been a Senior Research Engineer, Supervisor at NTT Network Innovation Laboratories. He is currently the Group Leader of a research group that develops millimeter-wave multi-gigabit wireless systems and software defined radios. Since March 2013, he has been a Guest Professor at Osaka University. From 2002 to 2005, he was an Associate Editor for the IEICE Transactions on Electronics. From 2004 to 2005, he was a Technical Program Committee member for the IEEE RFIC Symposium. Dr. Nakagawa is a Senior Member of the IEEE. He was the recipient of the 1995 Young Engineer Award presented by the IEICE.

Kazuhiro Uehara is a Senior Manager of the Wireless Systems Innovation Laboratory, NTT Network Innovation Laboratories. He received the B.E., M.E., and Ph.D. degrees from Tohoku University, Miyagi, in 1987, 1989, and 1992, respectively. In 1992, he joined NTT and engaged in research on array antennas, active antennas and indoor propagation in the millimeter-wave and microwave frequency bands. From 1997 to 1998, he was a Visiting Associate at the Department of Electrical Engineering, California Institute of Technology, USA. He was a part-time lecturer at the Department of Electrical Engineering, Tohoku University from 2003 to 2010, and at the School of High-Technology for Human Welfare, Tokai University from 2009 to 2011. His current interests include research and development of software defined radio and cognitive radio systems and millimeter-wave multi-gigabit wireless systems. From 2009 to 2011, he was Chair of the Technical Committee on Software Radio, TCSR, IEICE Communication Society. He was a General Co-Chair of the 6th International Conference on Cognitive Radio Oriented Wireless Networks and Communications, CrownCom, June 2011. He is a Guest Editor-in-Chief of the Special Section on Wireless Distributed Networks, and the Special Section on Cognitive Radio and Heterogeneous Wireless Networks in Conjunction with Main Topics of CrownCom2011, IEICE Transactions on Communications, December 2010 and April 2012, respectively. From 2011, he is an Adviser of the TCSR, IEICE. He received the Young Researcher's Award, Best Paper Award, Communications Society Outstanding Contributions Award, Communications Society Distinguished Contributions Award, and the Communication Society Best Paper Award from IEICE in 1995, 1997, twice in 2011, and 2012 respectively, the 1st YRP Award from the Yokosuka Telecom Research Park (YRP) R&D Promotion Committee, and the 18th Telecom System Technology Award from the Telecommunications Advancement Foundation in 2002 and 2003, respectively. He is a senior member of IEEE.